Materials Today Bio 32 (2025) 101638

Contents lists available at ScienceDirect

Materials Today Bio

journal homepage: www.journals.elsevier.com/materials-today-bio

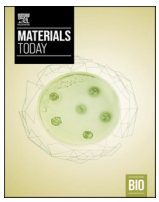

Bioinspired hydrogel for sustained minocycline release: A superior periodontitis solution

Shiyao Liu [a,1], Wenqian Zheng [b,c,1], Lina Wang [c,1], Yajie Zhang [a], Kang Feng [a], Yan Zhang [a], Haitao Yang [a], Yao Xiao [a], Chenxi Sun [c], Xiqiang Liu [a,*], Baoyang Lu [c,**], Xuemin Yin [a,***]

[a] Department of Stomatology, Nanfang Hospital, Southern Medical University, 1023 ShaTai South Road, Guangzhou, 510515, PR China
[b] Department of Pharmacy, Aerospace Center Hospital, 15 YuQuan Road, Beijing, 100049, PR China
[c] Jiangxi Provincial Key Laboratory of Flexible Electronics, Jiangxi Science and Technology Normal University, 605 FengLin Road, Nanchang, 330013, PR China

ARTICLE INFO

Keywords:
Periodontitis
Multifunctional hydrogels
Bioadhesive
Drug delivery
Periodontal regeneration
Minocycline

ABSTRACT

Periodontitis treatment remains challenging due to the limitations of clinical medication therapies, including drug cytotoxicity, poor drug retention, immune imbalances, and epithelial barrier damage. Here, inspired by bioisosterism, we develop a dual-network hydrogel-based drug delivery system (M@PP) with materials structurally similar to minocycline (a commonly used medication). The M@PP hydrogel exhibits optimal mechanical strength and bioadhesion, ensuring sufficient drug retention inside periodontal pockets. The sustained release of minocycline, combined with the hydrogel's acidic microenvironment and the antioxidant functional groups, provides M@PP with excellent biocompatibility, potent antibacterial activity (98.1 % against *P. gingivalis*), and enhanced anti-inflammatory properties. *In vivo* studies demonstrate that M@PP regulates macrophage polarization, upregulates anti-inflammatory factors, and promotes the expression of epithelial junction-related cytokines. Additionally, M@PP activates pro-osteogenic mediators, with micro-CT analysis revealing increased trabecular bone density, thickness, and bone reconstruction. RNA sequencing further uncovers its therapeutic mechanisms, highlighting bacterial defense, immune modulation and pro-regenerative signaling. These combined benefits create a favorable immune microenvironment, facilitating epithelial barrier restoration and alveolar bone regeneration, achieving superior therapeutic outcomes compared to commercial products. This study presents a promising localized therapeutic strategy for periodontitis and biofilm-associated disorders.

1. Introduction

Periodontitis, the third most prevalent non-communicable disease after cancer and cardiovascular disease, affects nearly 60 % of the global population [1,2]. This chronic condition is primarily caused by the imbalance of the oral microbiome-host immune homeostasis, contributing to progressive periodontal tissue destruction, even tooth loss [3]. Conventional treatments aim to eliminate bacterial biofilms through mechanical debridement coupled with local medications. However, these approaches often fail to achieve optimal therapeutic outcomes due to insufficient antibacterial efficacy, microbial recolonization, immunological imbalances, potential tissue damage[4–7]. Additionally, oral activities such as saliva flow can wash away the medication, further compromising the drug efficiency [8]. Combined with long-term follow-ups and heavy reliance on patient compliance, these limitations highlight the necessity for an advanced, sustained-release drug delivery system for periodontitis management.

Localized drug delivery systems (LDDSs) have emerged as promising strategies for improving periodontitis therapy by targeted drug release in the periodontal pocket, thereby enhancing drug bioavailability and minimizing the risks of antibiotic resistance and systemic side effects [9]. Among these, hydrogels with their high water content, biocompatibility, and porous scaffold structures have been extensively explored for delivering biological agents [10]. This biological agents include small-molecule drugs [11], growth factors [12], inorganic metals [13], nanoparticles [14], and protein-based drugs [15], aiming to achieve

* Corresponding author.
** Corresponding author.
*** Corresponding author.
E-mail addresses: liuxiqiang@smu.edu.cn (X. Liu), luby@jxstnu.edu.cn (B. Lu), yinxuemin1983@163.com (X. Yin).
[1] S.L., W.Z. and L.W. contributed equally to this work.

https://doi.org/10.1016/j.mtbio.2025.101638
Received 13 January 2025; Received in revised form 21 February 2025; Accepted 3 March 2025
Available online 12 March 2025

effective antibacterial properties and inflammation modulation. However, clinical translation is hindered by insufficient drug retention, potential intracellular toxicity, and the size- and dose-dependent limitations of nanoparticles [16]. In situ-forming hydrogels, while promising for periodontal applications, face challenges such as leakage and inflammatory responses caused by residual uncrosslinked components [17,18]. Furthermore, the high cost and lengthy development process of new biological agents further restrict their clinical application [9]. These challenges imply the urgent need for an optimized hydrogel system that ensures stable and sustained release of proven safe drugs, leading to superior therapeutic effects for periodontitis treatment.

Minocycline, widely used in periodontitis treatment for its antibacterial, anti-inflammatory, and tissue-regenerative properties, has limited localized application due to its high hydrophilicity, instability, and limited tissue penetration [19,20]. To address these limitations, bioinspired strategies offer a promising approach to enhance drug retention and therapeutic efficacy. Inspired by bioisosterism, a pharmacological strategy to enhance drug bioavailability and reduce side effects [21–23], we have developed a dual-network bioadhesvie hydrogel composed of poly(acrylic acid) (PAA) and poly(dopamine) (PDA), two biocompatible polymers that share structural similarities with minocycline [24,25]. These materials provide a stable drug-loading system via multiple molecular interactions, considerably enhancing drug loading capacity and release efficiency.

This study systematically evaluates the bioadhesion strength, mechanical stability, sustained drug release, antibacterial performance, and tissue-regenerative potential of the hydrogel *in vitro*, followed by *in vivo* validation in a periodontitis rat model to assess therapeutic efficacy and underlying healing mechanisms. By integrating bioinspired material design with targeted a well-accepted, FDA-approved drug delivery, this work has established a clinically translatable, cost-effective solution for superior periodontitis management.

2. Materials and methods

2.1. Materials

Acrylic acid (AA, >99 %), dopamine hydrochloride (DA·HCl, 98 %), N,N′-methylenebis(acrylamide) (MBAA, 99 %), ammonium persulphate (APS, 98 %), and sodium hydroxide (NaOH) were acquired from Aladdin (Shanghai, China). N,N,N′,N′-Tetramethylethylenediamine (TEMED, 99 %) was obtained from J&K Scientific (Beijing, China), and hydrochloric acid (HCl, 36–38 %) was purchased from Xilong Scientific (Shenzhen, China). Standard minocycline hydrochloride (minocycline, ≥98 %) was fetched from Solarbio (Beijing, China). All reagents applied in the experiments were analytical grade without further purification.

2.2. Fabrication of bioadhesive M@PP hydrogel system

The M@PP hydrogel system was composed of optimal adhesive and compressive poly(acrylic acid)-poly(dopamine) (PAA-PDA) hydrogel loaded with various minocycline hydrochlorides (0.05/0.1/0.2/0.4 mg mL^{-1}) by equilibrating in the minocycline solution.

2.2.1. Preparation of 1 wt% poly(dopamine) solutions

Dopamine hydrochloride (DA·HCl, 0.05 g) was dissolved in deionized water to prepare a 1 wt% dopamine solution, then 300 μL sodium hydroxide (NaOH, 12 mol L^{-1}) was instilled to adjust the pH value to alkaline. The 1 wt% dopamine solution was stirred constantly at room temperature and polymerized for 5–6 min until the color transformation, and the pH was transferred back with the same amount of HCl (12 mol L^{-1}) to terminate the polymerization process of dopamine.

2.2.2. Preparation of PAA-PDA hydrogels

Varying acrylic acid (AA) solution was prepared by blending different amounts of AA (6–14 g) with deionized water (9.65 mL), then mixed with previously mentioned 1 wt% dopamine solution (5 g), N,N′-methylenebis(acrylamide) (MBAA, 0.12 g), ammonium persulfate (APS, 0.2 g), and N,N,N′,N′-Tetramethylethylenediamine (TEMED, 40 μL) under vortex-mixing to obtain a homogeneous AA-PDA precursor solution (Solid content: 93.7/95.2/96.1/96.8/97.2 wt. PAA-PDA). Such a precursor solution was chemically crosslinked at 50 °C for 4 h to acquire a PAA-PDA (PP) hydrogel. Finally, we screened the optimal 96.1 wt% PP hydrogel according to its adhesive and compressive performances.

2.3. Characterization

SEM images of the hydrogel system were observed by a scanning electron microscope (SU8600, Hitachi). The mechanical characterizations of dumbbell-shaped and cylindrical hydrogels were severally evaluated by tensile and compressive tests [26] on a universal mechanical testing machine (WDW-01 with 0.1 kN load cell, Changchun Kexin). Fourier transform infrared spectroscopy (FT-IR) (Thermo Scientific, USA) was used to analyze the composition and chemical stability of hydrogels over time. Freeze-dried samples were collected in 15 d after fabrication and scanned four times within the 350-4500 cm^{-1} range to obtain the spectral data.

2.4. Adhesion performance

The adhesion performance of the PP hydrogel system was demonstrated by a standard lap-shear strength test with a universal mechanical testing machine (WDW-01 with a 0.1 kN load cell, Changchun Kexin) at a constant tensile speed of 15 mm min^{-1} (ASTM F2255) [27]. The influence of adhesive objects (tissue: porcine gingiva, heart, liver, skin, and muscle) (tissue engineering materials: glass, polyimide (PI), polyethylene terephthalate (PET), rubber, and titanium (Ti)) and water content (27 %–82.78 %) on adhesion performance was investigated in this work. The lap-shear strength (σ) of hydrogels was calculated by Equation (1):

$$\sigma = F_{max}/S \quad (1)$$

where F_{max} and S denote to the maximum force and the adhesive area, respectively.

2.5. Drug delivery performance

Drug-loaded efficiency of the hydrogel system was carried out by immersing the prepared PP hydrogel (~7.5 g, n = 3) in 20 mL of standard minocycline hydrochloride (0.05/0.1/0.2/0.4 mg mL^{-1}) for 24 h to ensure a balanced load. The M@PP hydrogel system was carefully removed and suspended over the drug solution for 2 min, allowing the loose surface solution to drip back into the solution. Then the remaining drug solution was configurated back to 20 mL with deionized water, and its absorbance was recorded at 350 nm by a UV–Vis–NIR spectrophotometer (TP-720, Specord 250 Plus). After the absorbance was converted to concentration by the concentration-absorbance standard curve, the drug-loaded efficiency (DLE) is determined by Equation (2):

$$DLE = (c_0\text{-}c_1) / c_0 \quad (2)$$

Where c_0 is the concentration of drug solution before hydrogel immersion; c_1 is the concentration of drug solution after hydrogel immersion.

Cumulative minocycline release was investigated by recording the minocycline content of dissolution medium (phosphate buffer saline, PBS) at 0.5, 1, 2, 3, 6, 12, 24, 36, 48, and 60 h. Fixing the M@PP hydrogel system between two disks of intelligent dissolving tester (ZRS-8GD, Tianda Tianfa) after the temperature of 500 mL dissolution medium (PBS, pH = 7.4) was maintained at 37 ± 0.5 °C with a constant speed of 100 r min^{-1}. Aliquots of 5 mL dissolution medium were collected from each dissolving cup at specific times for the subsequent absorbance test at 350 nm. Meanwhile, 5 mL PBS was added into the

system to keep a constant volume of dissolution medium.

2.6. Antimicrobial activity in vitro

2.6.1. Bacterial cultivation establishment of biofilms

Porphyromonas gingivalis and Fusobacterium nucleatum (gram-negative bacterium, *P. gingivalis*, ATCC 33277, USA, and *F. nucleatum*, ATCC 25586, USA) were considered keystone pathogen and bridging bacterium in dental plaque [28], respectively, cultured with brain heart infusion (BHI, Sigma-Aldrich, USA) agar plate supplemented with hemin (0.5 mg L^{-1}, Solarbio, China), vitamin K1 (0.1 mg L^{-1}, Solarbio, China), and 5 % defibrinated sheep blood (Solarbio, China) at 37 °C anaerobically. Streptococcus gordonii (gram-positive bacterium, *S. gordonii*, Challis CH1), generously provided by Guangdong Provincial Key Laboratory of Stomatology, Sun Yat-sen University, commonly colonizes newly cleaned teeth, aiding biofilm formation by facilitating attachment of other oral pathogens [29], was cultured aerobically in freshly prepared BHI broth. The inoculum concentration of *S. gordonii* was adjusted to 1×10^6 colony forming units (CFU) mL^{-1}, and the cultures of *P. gingivalis* and *F. nucleatum* were diluted to 1×10^7 CFU mL^{-1} for future testing and biofilm formation.

2.6.2. Antibacterial tests against plantonic bacteria

The antimicrobial capability of PP and M@PP hydrogels was tested using BHI liquid cultures and agar plates assays. BHI medium and minocycline hydrochloride ointment (MHO, Periocline®) were selected as negative controls and positive controls, respectively. The hydrogel was sterilized by UV light irradiation before bacterial cultures [30] and all the tests were conducted under BHI medium with the tested PP hydrogel and M@PP hydrogel containing minocycline concentrations of 50, 100, 200, and 400 μg mL^{-1} (M-0.5@PP, M-1@PP, M-2@PP, and M-4@PP). The mixture of 5 mL bacteria suspension in BHI medium and 2 mg PP or M@PP was incubated in a 37 °C shaker at 160 RPM for 24 h, 48 h, and 72 h, according to the American Society of Testing Materials (ASTM) standards E2149. The optical density (OD) at 600 nm of BHI medium was measured at different time intervals on a micro-plate reader (a SpectraMax M2 Multimode Microplate Reader). The antibacterial killing ratio of bacteria was calculated using the following equation (3):

$$\text{Antibacterial ratio } (\%) = [(OD_a\text{-}OD_b) / OD_a] \times 100\ \% \quad (3)$$

where OD_a and OD_b represent the OD value of the control group and the experimental group, respectively.

100 μL *P. gingivalis*, *F. nucleatum*, or *S. gordonii* suspension was dispersed on the surface of PP and M@PP hydrogels (disc-shaped; thickness 1 mm, diameter 5 mm) and cultivated at 37 °C for 24 h under anaerobic conditions. Then, 100 μL of treated bacterial suspensions (10^{-4} times diluted) were equally distributed on sterilized BHI blood agar plates. After 7 d of incubation at 37 °C, the forms of bacterial colonies were photographed for record.

2.6.3. Antibiofilm activities of M@PP hydrogel

500 μL of the representative major periodontal pathogen *P. gingivalis* was selected to construct monospecies biofilms, or 500 μL of *S. gordonii, P. gingivalis,* and *F. nucleatum* were implanted at 1-h intervals to build multispecies biofilms in confocal dishes. After co-culturing the samples (disc-shaped; diameter 6 mm, thickness 1 mm) with dental plaque biofilms for 1 d, the samples were stained with a microbe viability staining kit (Invitrogen, Themo Fisher Scientific, USA), with 2.5 μM SYTO 9 (green for active bacteria) mixed with an equal amount of PI dye (red for dead bacteria) according to the recommended procedures. Biofilm inhibition was visualized using confocal laser scanning microscopy (Olympus 141 FV3000).

The quantification of biofilm disruption was assessed using the crystal violet assay. Multi-species dental plaque biofilms were established on hydroxyapatite (HA) slices (disc-shaped; 2 mm thick, 10 mm in diameter) pre-coated with artificial saliva for 24 h. Afterward, the samples were placed on the HA slices and co-cultured under stationary conditions for an additional 24 h under anaerobic conditions. Then HA slices were rinsed three times in sterile PBS to remove extra planktonic cells. The resulting biofilms were fixed with 95 % methanol and stained with 1 mL 1 % (w/v) crystal violet solution (Solarbio, Beijing, China), then crystal violet was released by adding 33 % acetic acid and subjected to microplate reader at an absorption of 590 nm. Every treatment was performed at least four times. The percentage of inhibition was calculated by equation (4):

$$\text{Inhibition ratio } (\%) = (1\text{-}OD_a / OD_b) \times 100\ \% \quad (4)$$

Where OD_a and OD_b represent the OD values of the experiment and the blank group, respectively.

2.7. Biological assay in vitro

Mouse calvaria-derived preosteoblastic cell lines (MC3t3-E1s; ATCC, USA) were grown in Dulbecco's modified Eagle's medium (DMEM, Gibco, MD) containing 1 % (v/v) penicillin (Hyclone, USA), 1 % (v/v) streptomycin (Hyclone, USA), and 10 % fetal calf serum (Gibco, MD). Human immortalized oral epithelial cell lines (HIOECs; ATCC, USA) were grown in Keratinocyte Serum Free Medium (KSFM, Thermo Fisher Scientific, USA) with antibiotics (1 % (v/v) penicillin and 1 % (v/v) streptomycin; Hyclone, USA).

2.7.1. Cytocompatibility assay

Cell Counting Kit-8 (CCK-8, Dojindo, Japan) test was employed to assess cell proliferation, utilizing hydrogel extracts at different concentrations. To generate the conditioned medium, 100 mg of MHO, PP, and M@PP hydrogel were incubated in 5 mL of DMEM or KSFM at 37 °C for 24 h [31]. Subsequently, sample extracts (20 mg mL^{-1}) were diluted with the medium to produce leaching solutions at concentrations of 5 mg mL^{-1} and 1.25 mg mL^{-1}, enabling a comprehensive evaluation of cytocompatibility. For MC3T3-E1 and HIOEC viability assays, cells were seeded in 96-well plates at densities of 2×10^3 cells per well and 6×10^3 cells per well, respectively, and incubated for 24 h before exposure to the hydrogel extracts. To compare the cytocompatibility of different hydrogel formulations, a CCK-8 assay was conducted using a standardized hydrogel extract concentration of 5 μg mL^{-1} testing MHO, PP, M-0.5@PP, M-1@PP, M-2@PP, and M-4@PP groups. To investigate the dose-dependent effects of hydrogel extracts, another CCK-8 assay was performed with sample extract concentrations of 1.25, 5, and 20 μg mL^{-1}, comparing MHO, PP, and M-4@PP groups. After 24 and 48 h, 10 μL of CCK-8 solution was added to each well, incubated for 2 h, and the absorbance at 450 nm was measured using a microplate reader (SpectraMax i3x, Molecular Devices, USA). Additionally, to further evaluate the potential cytotoxicity of pure minocycline solution, HIOECs were co-cultured with different concentrations of minocycline solution for 24, 48, and 72 h. The relative cell viability was estimated using the following equation (5):

$$\text{Cell viability } (\%) = [(OD_a\text{-}OD_c) / (OD_b\text{-}OD_c)] \times 100\ \% \quad (5)$$

where OD_a and OD_b represent the OD values of the experimental group and the control group, respectively, and OD_c is the OD value of the blank group (supplemented with standard medium and CCK-8 solution).

2.7.2. Flow cytometry

HIOECs were seeded into 6-well plates and incubated overnight. After 24 h of co-culturing with varied doses of minocycline solution, the treated cells were harvested and prepared as single-cell suspensions using an appropriate trypsin cell digestion solution. After centrifugation, add 5 μL of Annexin V-FITC and 10 μL of propidium iodide staining solution, gently mix, and incubate in the dark for 10–20 min before flow

cytometry analysis (MoFlo XDP, Beckman, USA). And the analysis was conducted using FlowJo software (FlowJo LLC, USA).

2.7.3. Live/dead assay

After 24 and 48 h of co-incubated with leaching solutions at concentrations of 5 mg mL^{-1}, HIOECs and MC3T3-E1s were stained using the Calcein-AM and PI live-dead cell staining kit (Beyotime, China). To label live cells in green and dead cells in red, add the staining solution to the cells and incubate for 30 min, as per the instructions. Subsequently, the images were examined with an inverted fluorescence microscope (Nikon TE 2000-U, Japan).

2.7.4. Scratch wound assay

After MC3t3-E1s were planted in a 6-well plate (1×10^5 cells per well) and incubated in FBE-free medium. A sterile 200 μL pipette tip was used to make a scratch across the monolayer. The floating debris was washed three times with PBS. For the control group, DMEM (without serum) medium was added, hydrogel extract solution (5 mg mL^{-1}) was utilized as the experimental group. After 24 and 48 h, the scratch changes were examined with a light microscope (BX 63, Olympus Corporation, Japan) and the regrowth of the wounded areas was measured. Three scratch wounds were assessed per well, and migration healing rate was calculated using the following formula (6):

$$\text{Cell migration}\ (\%) = [(S_a\text{-}S_b) / S_a] \times 100\ \% \quad (6)$$

where Sa and Sb represent the scratch area at 0 h and the designated time, respectively.

2.7.5. Quantitative real-time reverse transcription PCR (qRT-PCR)

Total RNA was isolated from cells cultured either with MHO or hydrogel groups for 14 d, employing the RNA-Quick Purification Kit (Yishan Biotechnology, China). Subsequently, reverse transcription to cDNA was accomplished using the HiScriptIII All-in-one RT SuperMix for quantitative PCR (Vazyme Biotech, China). Taq Pro Universal SYBR qPCR Master Mix (Vazyme Biotech, China) was used for qRT-PCR analysis, with cDNA as the template, following manufacturer instructions. The primer sequences used in this work are presented in Supplemental Table S2.

2.8. Animal experiments

The *in vivo* rat periodontitis model and experimental design followed procedures and regulations authorized by Southern Medical University's Animal Use and Care Committee and Medical Ethics Committee (Permit number: IACUC-LAC-20231019-002). In this study, a total of 6-week-old, 80 male, Sprague-Dawley specific pathogen-free (SPF) rats were utilized to verify the therapeutic efficacy of M-4@PP hydrogel implantation. Under general anesthesia, a 4-0 silk suture was gently placed around the upper right first molar without causing any mechanical damage to the surrounding periodontal tissue, following 7 d of culture adaptation. To induce periodontitis, rats were fed with 10 % sugar water, and a 400 μL suspension of *F. nucleatum* and *P. gingivalis* was introduced one day after the initial colonization of *S. gordonii* for each rat at one-day intervals. The ligatures were checked daily to ensure they remained in place for 2 w. Rats were then divided into three groups (20 rats per group): Saline, MHO, and M-4@PP hydrogel. After removing the dental biofilms around the first maxillary molars and performing constant saline irrigation, the disinfected M-4@PP hydrogel was inserted into the lingual defect sites [32], while the MHO group was inserted weekly into the periodontal pockets according to the manufacturer's instructions. All operations were performed by the same operator and at each time point (days 2, 7, 14, and 28 post-operation), 5 rats from each group were randomly sacrificed to evaluate the periodontal pathogens' defense, anti-inflammatory, and osteogenic properties. To test the antibacterial activities against microorganisms, periodontal pathogens from each group were obtained two-day post-treatment for bacterial culture.

2.8.1. Transcriptome sequencing and data analysis

Gingiva tissues were extracted from rats with periodontitis that had been treated with saline or M-4@PP hydrogel for 7 d. RNA samples were extracted and analyzed with a NanoDrop and an Agilent 2100 bioanalyzer (Thermo Fisher Scientific, MA, USA). Transcriptome sequencing libraries were created, and data analysis was performed using the Dr. Tom System (https://biosys.bgi.com/).

2.8.2. Enzyme-linked immunosorbent assay (ELISA)

Whole blood was collected using EDTA as an anticoagulant in rats, then centrifuged for 15 min on postoperative days 2 and 7. After that, an ELISA assay of rat tumor necrosis factor α (TNF-α) was conducted using an ELISA kit (JINGMEI Biotechnology, Jiangsu, China) following the manufacturer's protocol.

2.8.3. Analysis of gingival tissue samples by Western Blotting

After 14 d of sample treatment, periodontal soft tissues around the first molar were harvested, and total proteins were extracted using Radioimmunoprecipitation assay (RIPA) lysis buffer (Beyotime, Jiangsu, China) to determine whether or not the gingival tissue barrier functioned. Incubated membranes with ZO-1, E-cadherin antibody (Proteintech, Chicago, USA) for target protein or β-actin antibody (Proteintech, Chicago, USA) for reference after protein determination by a BCA Protein Assay Kit (Beyotime, Shanghai, China), loaded on SDS-PAGE gel and been electrophoretically transferred, protein bands were visualized with an Odyssey Fc System (LI-COR, Lincoln, USA) and analyzed using Image J software.

2.8.4. Imaging examination and histological analysis

Gingival inflammation and periodontal tissue remodeling were tracked over time using photographic recording. The hard tissue, including maxillary molar teeth and alveolar bone beneath, was fixed with 10 % paraformaldehyde and analyzed using a high-resolution X-ray microtomography system (Skyscan 1172, Bruker, Belgium). In order to assess the vertical bone defect, the distances between the Alveolar Bone Crest (ABC) and the Cemento-Enamel Junction (CEJ) were measured three times at each of the six first-molar sites (disto-buccal, mid-buccal, mesio-buccal, disto-palatal, mid-palatal, and mesio-platal). Micro-CT analysis was performed with scanning parameters set at 65 kV, 385 μA, 15.38 μm resolution, and 35 min exposure. Reconstructed images were processed using NRecon and CT-Analyzer software (Bruker, Kontich, Belgium), with region of interest (ROI) selection standardized based on anatomical landmarks. The first maxillary molar region was chosen for analysis. A constant rectangular ROI was applied across all samples, spanning 150 slices, with the length was determined from the distopalatal root surface of the first maxillary molar to the mesiopalatal root surface of the second maxillary molar on mesio-distal sagittal slices, while the width extended from the palatal side to the buccal-palatal root furcation on coronal segmentation planes. All root volumes were excluded to ensure accurate calculation of bone parameters (BV/TV, Tb. N, Tb.Sp) at the fourth week post-treatment, and ROI placement was independently verified to ensure consistency.

The periodontal site and adjacent normal tissue were obtained and sectioned for Hematoxylin and Eosin (H&E) and Immunohistochemistry to further confirm the process of the pathological changes of the periodontal tissues and subsequent periodontal bone regeneration. Quantitative analysis was carried out using the Image J software mentioned above. Furthermore, H&E staining was performed on the major organs, including the heart, liver, lung, kidney, and spleen, and blood samples from rats were taken for toxic testing at 28 days post-implantation to assess the biocompatibility of the M-4@PP hydrogels.

Statistical analysis was performed utilizing GraphPad Prism 9.5.1 (GraphPad Software Inc., San Diego, CA, USA), with all data reported as

means ± S.E.M. The Shaprio-Wilk test was applied to confirm the normal distribution of the data. The *t*-test and one-way analysis of variance (ANOVA) were used to determine significant differences (*$p <$ 0.05, **$p < 0.01$, ***$p < 0.001$, and ****$p < 0.0001$).

3. Results and discussion

3.1. Design and fabrication of M@PP hydrogel

Periodontitis-related pathogens play a critical role in the formation of dental plaque and the disruption of oral microbiome-host immune balance, leading to inflammation and periodontal tissue destruction (Fig. 1a). Aiming for highly efficient and cost-effective periodontitis therapy, we are inspired by the principles of bioimmune rejection [22], selecting materials structurally similar to minocycline as a drug delivery platform (Fig. 1b). This strategy not only enhances the loading and utilization of minocycline (Fig. 1c), but also promotes a favorable immune environment to achieve periodontal regeneration (Fig. 1d).

The drug delivery platform consists of an interpenetrating double-network hydrogel made from polydopamine (PDA) and poly(acrylic acid) (PAA). The hydrogel, rich in hydroxyl and carboxyl groups, ensures effective adhesion in the moist periodontal environment [24,25] while providing a physical barrier against external pressures and pathogens (Fig. 1e). Additionally, the dense hydroxyl and carboxyl groups serve as natural antioxidants, helping reduce the risk of infection at the wound spot [33,34]. Importantly, PAA is an FDA-approved biocompatible material [35], which guarantees the excellent biocompatibility of the delivery platform. To balance the relationship between the mechanical strength of the hydrogel and its surface adhesion [36,37], we optimize the ratio of PAA to PDA to achieve an ideal formulation for sustained drug release (Fig. 1f–S1-2). This controlled release of minocycline minimizes the risk of cytotoxicity, which is crucial for maintaining the host-microbiome balance, ultimately promoting the healing of periodontal soft and hard tissues (Fig. 1g).

As a drug-controlled release platform, the on-demand release of minocycline is crucial. This hydrogel-based delivery system composed of materials structurally similar to minocycline enhances high drug loading efficiency. The interpenetrating double-network hydrogel interacts with minocycline through hydrogen bonding, electrostatic forces, and physical absorption, creating spatial constraints (Fig. 1h) that ensure the slow and sustained release of the drug. Sustained minocycline release from this three-dimensional network (Fig. S3) is diffusion-dependent, determined by the interaction between the drug's hydrodynamic diameter and the network mesh size [38] (Fig. 1h). The PAA-PDA (PP)

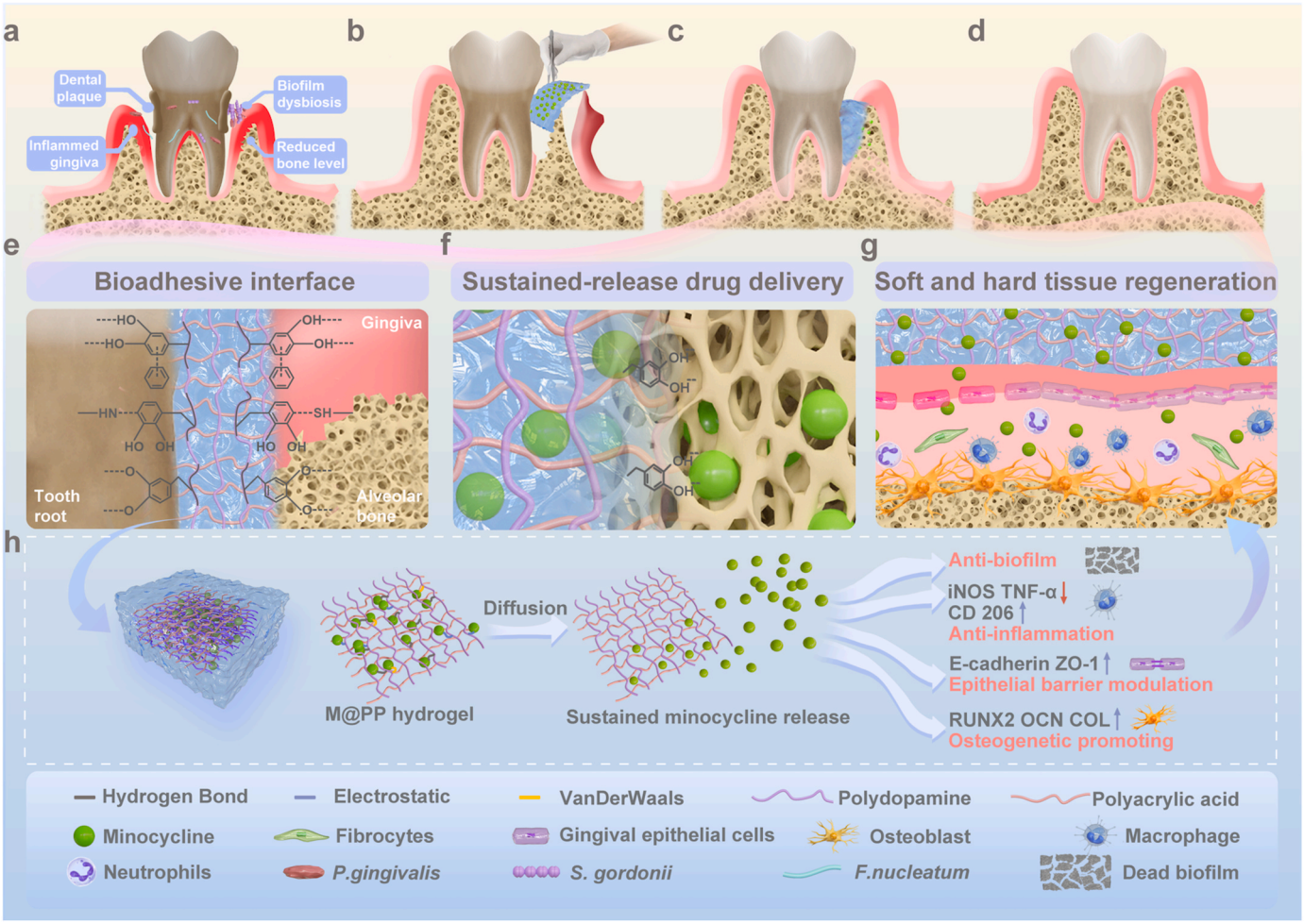

Fig. 1. Schematic illustration of the bioadhesive drug-loaded hydrogel for periodontitis treatment.
(a–d) The application of minocycline-loaded poly(dopamine)-poly(acrylic acid) (M@PP) hydrogel for periodontitis (a). After being fabricated, this dual-network bioadhesive M@PP hydrogel is inserted into the periodontal pockets (b). It maintains a supportive immunological environment and sustained minocycline administration (c), achieving periodontal regeneration (d). (e–g) M@PP hydrogel could firmly adhere to tooth surfaces and periodontal tissues (e), allowing stable, localized medication release (f), thus encouraging periodontal soft and hard tissue healing (g). (h) This double-network hydrogel interacts with minocycline through hydrogen bonding and electrostatic forces, resulting in sustained drug release that can eradicate pathogenic microorganisms, reduce pro-inflammatory factors, and accelerate the expression of osteogenesis genes and epithelial barrier recovery, thereby promoting effective periodontal regeneration.

hydrogel creates a slightly acidic microenvironment that enhances minocycline stability and optimizes therapeutic efficacy, while the antioxidant effect of its functional groups ensures the drug-carrying platform excellent anti-inflammatory effect [39,40].

This multifunctional hydrogel is designed to effectively target and eliminate periodontitis-related pathogens at non-toxic minocycline concentrations, demonstrating efficient anti-biofilm activity. Furthermore, by modulating macrophage polarization and enhancing the expression of genes and proteins related to osteogenesis and epithelial junctions, this multifunctional composite demonstrates significant anti-inflammatory effects, promotes epithelial barrier modulation, and supports osteogenetic promoting (Fig. 1h). This cost-effective hydrogel supports periodontal regeneration by repairing the defensive barrier and balancing the periodontal microbiome-host interaction, resulting in a synergistic effect known as "1 + 1>3,", which outperforms commercially available medicines.

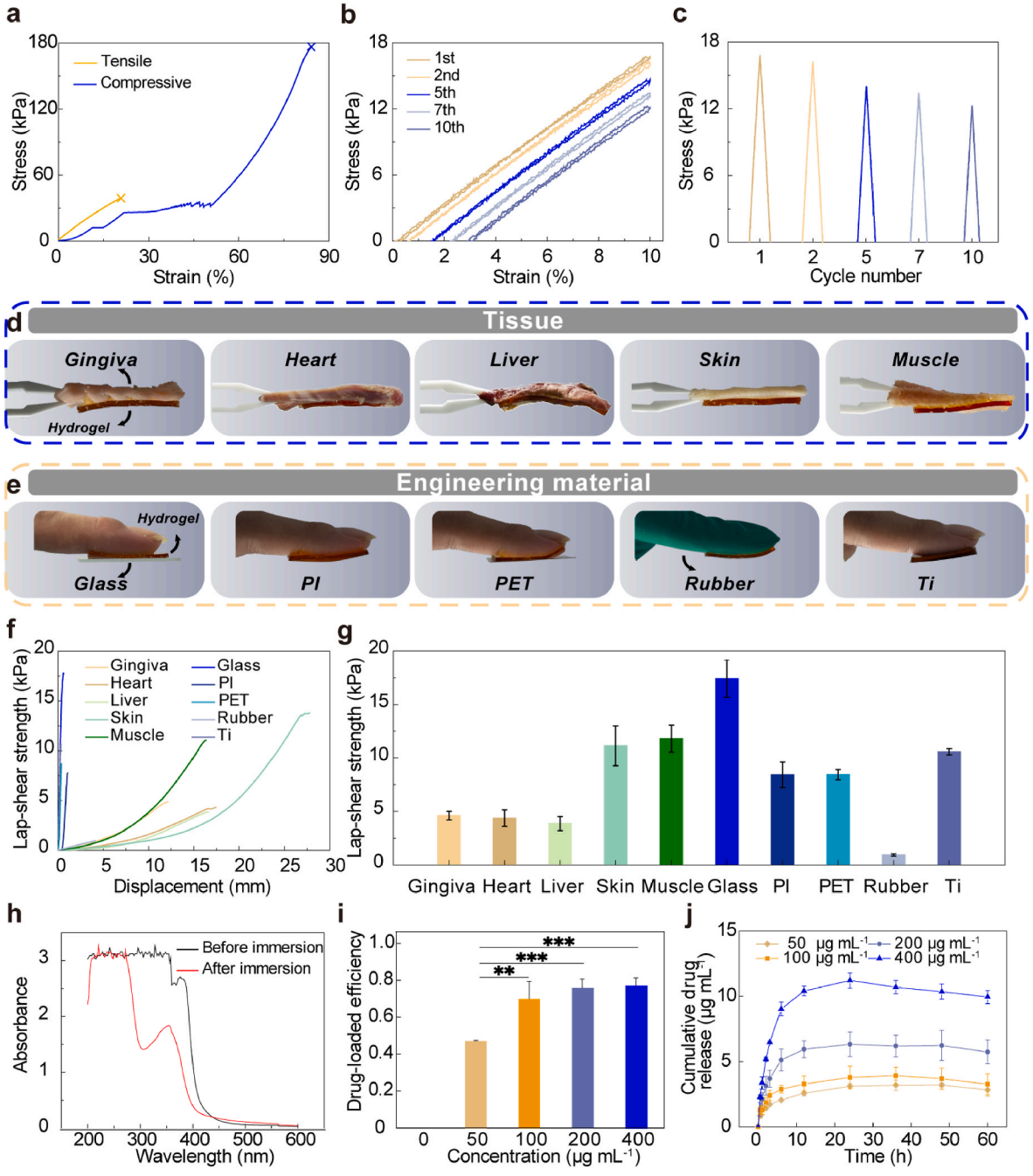

Fig. 2. Mechanical properties, adhesion performance, and drug release of poly(acrylic acid)-poly(dopamine) (PP) and minocycline-loaded PP (M@PP) hydrogel. (a) Tensile and compressive stress-strain curves of PP hydrogels (96.1 wt% poly(acrylic acid)). (b) Cyclic stress–strain curves of PP hydrogels under the strain of 10 %. (c) Stress variation of PP hydrogels at 1st, 2nd, 5th, 7th and 10th cycles. (d–e) Photos showing adhesive effects of PP hydrogels adhering to various substrates (porcine gingiva, heart, liver, skin, muscle, glass, PI, PET, rubber and Ti). (f) Representative stress-displacement curves of lap shear strength tests between PP hydrogels and various substrates. (g) Shear strength of PP hydrogels adhering to various substrates by lap-shear test (n = 3). (h) UV–Vis absorption spectrum of PP hydrogel and M@PP hydrogel. (i) Drug loading efficiency of M@PP hydrogel at different minocycline concentrations (n = 3). (j) The cumulative amounts of minocycline released from M@PP hydrogel at 0–60 h (n = 3).

3.2. Mechanical properties, adhesion performance, and drug release of M@PP hydrogel

3.2.1. Mechanical properties and adhesion performance

An ideal biological drug-carrying material for treating periodontitis should possess sufficient elasticity and adhesion to adapt to the dynamic environment in the oral cavity. We employ poly(dopamine) (PDA) as an adhesive system, and optimize the integrated mechanical-adhesion properties of PAA-PDA hydrogels (96.1 wt% PAA) by modulating the mass ratio of poly(acrylic acid) and poly(dopamine) (Figs. S1–2). Upon compression and stretching, PAA-PDA (PP) hydrogel displays a satisfactory compressive and tensile strength of 177.2 kPa and 39.08 kPa (Fig. 2a), respectively, perfectly accommodating to the strength range of the oral cavity. The tensile Young's modulus of hydrogel has been calculated to be 212.1 kPa, to guarantee its exceptional mechanical compatibility with teeth and periodontal tissues. Moreover, hydrogel's continuous strain-stress cycling at a strain of 10 % indicates the material's exceptional mechanical stability by preserving 73.2 % of its maximum stress after 10 cycles (Fig. 2b–c). The characteristic peaks of the polymer at 3453, 1596, and 1355 cm^{-1} remain unchanged after 15 d, exhibiting sufficient stability for practical use over an extended period (Figs. S4–5).

Meanwhile, achieving a stable bioadhesive interface between the tooth and tissue is crucial for a stable connection of the drug-carrying platform to the periodontal pockets. We have systematically explored the adhesion properties of PP hydrogels with tissues (porcine gingiva, heart, liver, skin, and muscle) and engineering materials (glass, polyimide (PI), polyethylene terephthalate (PET), rubber, and titanium (Ti)) (Fig. 2d–e). The lap-shear strength of PP hydrogels with varied water content (27 %–82.8 %) on the porcine gingiva decrease from 2.07 kPa to 0.50 kPa, proving the prominent bioadhesive stability of hydrogel in moist oral environment (Fig. S6). The excellent bioadhesive strength of PP hydrogel on gingiva, skin, and muscle was 4.61 kPa, 11.13 kPa, and 11.80 kPa, respectively, while the adhesion strength of glass and Ti was 17.40 kPa and 10.57 kPa (Fig. 2f and g). Notably, PP hydrogel demonstrates a relatively high bioadhesive-mechanical strength in comparison with other previously reported oral hydrogels (mechanical: 54–300 kPa, adhesive: 5.3–38.72 kPa) and gels/injectable hydrogels (mechanical: 5.3–168 kPa, adhesive: 3.6–16.46 kPa) (Table S1). These excellent adhesion findings are due to the hydrogel's abundance of functional groups, particularly catechol and amino groups [41]. In addition, various non-covalent interactions can be formed between the PP hydrogel and the substrate, including ion-dipole, hydrogen bonding, and metal-ligand bonding (Fig. 1e). Overall, PP hydrogel exhibits appreciable mechanical and adhesive performances for the subsequent stable minocycline delivery systems against dynamic oral environment, potentially restoring the disrupted oral epithelial barrier to promote the recovery of periodontal tissues.

3.2.2. Drug release profile of M@PP

To address challenges such as burst drug release, epithelial cell sensitivity to minocycline, and potential homeostasis disruption, we select a porous PAA-PDA (PP) hydrogel that is structurally similar to minocycline, as a local drug delivery strategy. A characteristic absorption peak at 352 nm confirms successful minocycline loading (Fig. 2h). While higher concentrations improve encapsulation efficiency, statistical analysis shows no significant differences among M-1@PP (100 μg mL^{-1}, 70.1 %), M-2@PP (200 μg mL^{-1}, 76.2 %), and M-4@PP (400 μg mL^{-1}, 77.3 %), whereas M-0.5@PP (50 μg mL^{-1}, 47.4 %) is significantly lower (**$p < 0.01$, ***$p < 0.001$) (Fig. 2i). Thus, increasing minocycline beyond 100 μg mL^{-1} does not further enhance hydrogel performance. The drug release mechanism is primarily governed by concentration gradient diffusion and further modulated by drug-polymer interactions [38], allowing for sustained minocycline release at the target location. M-4@PP exhibits the highest minocycline release, with an initial phase within the first 10 h, followed by a controlled and sustained release, maintaining a therapeutic concentration (~10 μg mL^{-1}) for up to 60 h (Fig. 2j).

This extended release profile ensures prolonged antibacterial efficacy while minimizing potential toxicity. Our research (Fig. S7) indicates that minocycline concentrations above 200 μg mL^{-1} induce necrosis and apoptosis in approximately 50 % of oral epithelial cells, whereas lower concentrations (25 μg mL^{-1}) maintain high cell viability (110.64 % after 72 h). Importantly, the maximum concentration released from M-4@PP never exceeds 15 μg mL^{-1} (Fig. 2j). While commercial minocycline formulations such as Periocline® exhibit an initial burst release exceeding 1300 μg mL^{-1}, which may cause severe cytotoxic effects and disruption of periodontal tissues [42]. The M@PP hydrogel effectively optimizes minocycline delivery, achieving a prolonged, non-toxic, and bactericidal concentration, thereby enhancing antimicrobial efficacy while minimizing adverse effects.

3.3. Antimicrobial capabilities of M@PP in vitro

3.3.1. Antibacterial efficiency of PP and M@PP against planktonic bacteria

To assess the antibacterial efficacy against periodontal planktonic pathogens, M@PP hydrogel has been compared with minocycline hydrochloride ointment (MHO), a clinically utilized antimicrobial agent. The drug-loaded hydrogels exhibit dose-dependent antimicrobial activity due to the steady release of minocycline, while MHO groups partially inhibit bacterial growth (Fig. 3a, S8). Specifically, the 72 h bacterial-killing ratios achieved with M-0.5@PP (hydrogel loaded with 50 μg mL^{-1} of minocycline) to M-4@PP (hydrogel loaded with 400 μg mL^{-1} of minocycline) hydrogels are 95.1 %–98.1 % for *P. gingivalis* (Figs. 3b), 92.6 %–95.5 % for *F. nucleatum* (Figs. 3c), and 92.8 %–95.3 % for *S. gordonii* (Fig. 3d), all notably higher than those achieved with MHO (88.1 %, 80.8%, and 61.3%, respectively). Additionally, the PP hydrogel maintain strong antibacterial effects over 72 h, with bacterial-killing rates of 93.8 % for *P. gingivalis*, 90.5 % for *S. gordonii*, and 89.4 % for *F. nucleatum* (Fig. 3b–d). This enhanced performance has generally been attributed to the catechol structure of PDA, which disrupts bacterial metabolism, and protonated amine groups that interact with bacterial cell walls, causing their breakdown [43,44]. The three-dimensional network structure provides a larger surface area, capturing and immobilizing periodontal microorganisms, effectively restricting bacterial migration and proliferation [45,46]. Additionally, BHI agar plate results (Fig. 3e) visually corroborate the PP hydrogel's enhanced antibacterial efficacy, with the M-4@PP hydrogel displaying the fewest colonies, highlighting the advantage of combining inherent antimicrobial properties with controlled minocycline release from the porous network.

3.3.2. Enhanced anti-biofilm performances of M@PP

Disrupting dental plaque biofilms and preventing their reformation are crucial for controlling the progression of periodontal disease. While MHO shows some inhibitory effects on *P. gingivalis* single-species biofilms, its antimicrobial efficacy declines as the biofilm transitions from single to multi-species (Fig. 3f). Additionally, 3D confocal imaging (Fig. 3f) reveals that untreated multi-species biofilms are significantly thicker than single-species biofilms, exceeding 40 μm, suggesting that complex bacterial interactions promote biofilm growth. These interactions enable bacteria to utilize diverse metabolic pathways and secrete protective extracellular substances, increasing biofilm resistance to environmental challenges, like local antibiotics, which may reduce drug efficacy [28,47]. In contrast, the M-4@PP group exhibits the highest proportion of dead bacterial cells and significantly thinner biofilms, outperforming both the MHO and PP hydrogel groups in biofilm inhibition.

To better mimic actual oral scenarios and further validate the M@PP's ability to disrupt multi-species biofilms, *S. gordonii, F. nucleatum,* and *P. gingivalis* have been inoculated on hydroxyapatite discs treated with artificial saliva, simulating the progressive colonization of

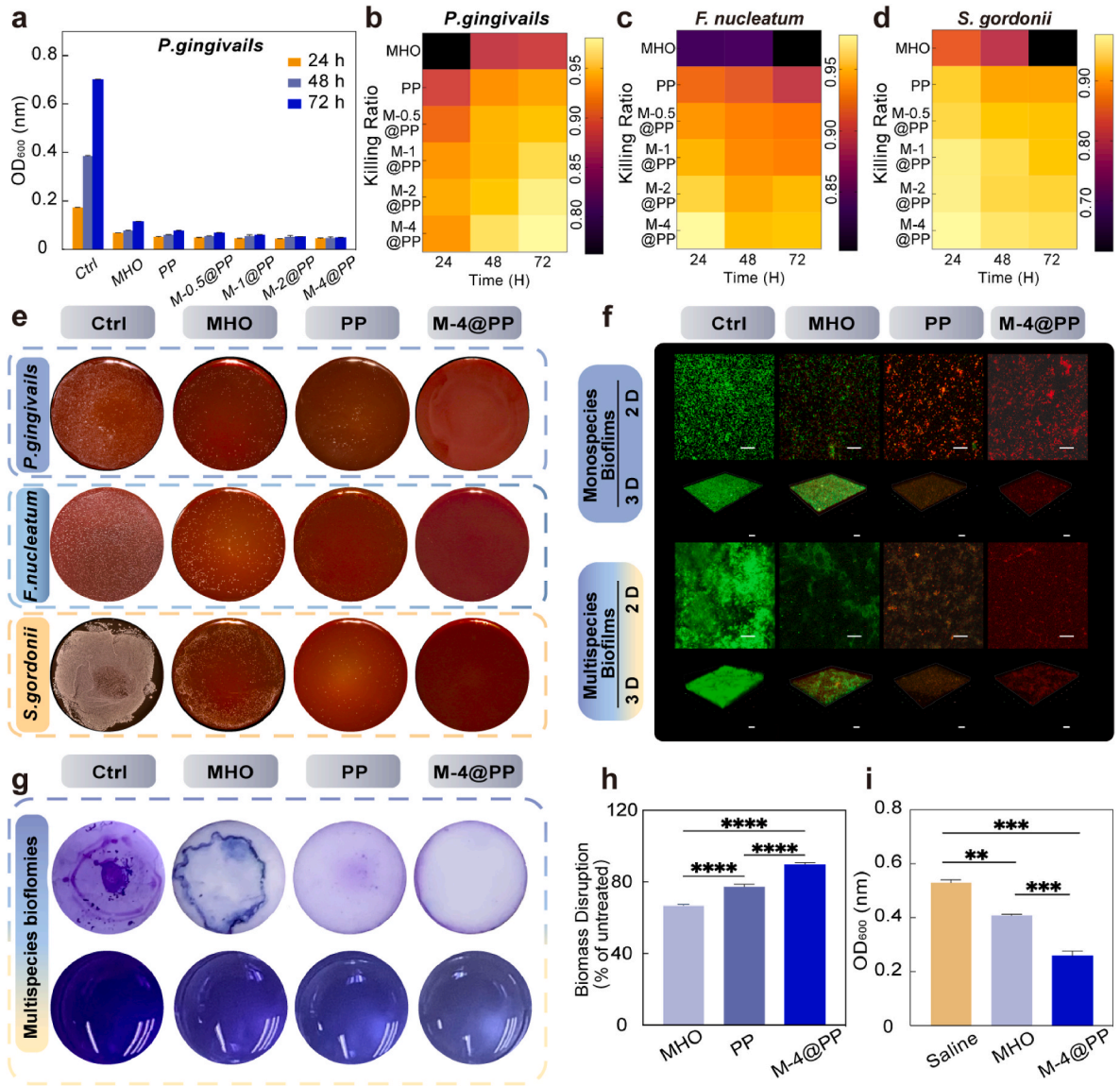

Fig. 3. Antimicrobial capabilities of M@PP *in vitro* and *in vivo*
(a) The optical density of *P. gingivalis* in the presence of MHO (a clinically utilized minocycline ointment, positive control), PP hydrogel, and M@PP hydrogel containing minocycline concentrations of 50, 100, 200, and 400 μg mL^{-1} (M-0.5@PP, M-1@PP, M-2@PP, and M-4@PP) at 600 nm (OD_{600}) (n = 5). (b–d) Killing ratios of *P. gingivalis, F. nucleatum,* and *S. gordonii* according to the OD_{600} (incubated with the hydrogels extracts for 72 h). (e) Digital photographs of corresponding colony-forming units (CFU) of different co-cultured bacterial cultures (7 d incubation on BHI agar plates, against *P. gingivalis, F. nucleatum,* and *S. gordonii* (n = 5)). (f) Representative live/dead images of monospecies and multispecies biofilms for bacterial viability detection, with live bacteria stained green and dead bacteria stained red (n = 3). Scale bar: 25 μm in 2D images and 50 μm in 3D images. (g) Biofilm destruction is assessed by incubating the MHO, PP and M-4@PP hydrogels with pre-formed multispecies bacteria in BHI for 24 h, discarding the BHI media and staining the adhered biomass with crystal violet. (h) The percentage of biofilm disruption in the treated groups is quantified relative to the untreated group, which is set as 0 % (n = 4, $^{****}p < 0.0001$). (i) Corresponding optical density of oral bacterial in biofilms on rats' teeth treated with various treatments at 600 nm (OD_{600}) (n = 5, $^{**}p < 0.01$, and $^{***}p < 0.001$). (For interpretation of the references to color in this figure legend, the reader is referred to the Web version of this article.)

periodontal bacteria on the tooth surface. The PP hydrogel significantly disrupts pre-formed multispecies biofilms by 77.26 % compared to the untreated group (0 %) (Fig. 3g–h). Moreover, the M-4@PP hydrogel demonstrates the highest biofilm disruption efficiency (89.62 %) on multispecies biofilms, significantly surpassing the MHO group (66.63 %) ($^{****}p < 0.0001$) (Fig. 3g–h). These results suggest that the hydrogel's strong tissue adhesion enables sustained minocycline release at target sites, effectively disrupting established biofilms and preventing bacterial recolonization.

3.4. *Effects of the M@PP hydrogel on cytocompatibility and bioactivity in vitro*

Given that the material will be inserted into the periodontal pocket and come into direct contact with the gingival epithelium and alveolar bone, we select HIOECs and MC3t3-E1s to assess the biosafety of M@PP hydrogel. Live/dead assay imaging (Fig. 4a and c) reveals that the majority of the spindle-shaped MC3t3-E1s and cobblestone-like cuboidal-shaped HIOECs stained green (live cells), with almost no red-stained dead cells, exhibiting satisfactory time-dependent growth. Both PP and M@PP hydrogels demonstrate excellent biocompatibility. The cell viability of MC3t3-E1s and HIOECs exposed to leaching solutions of PP,

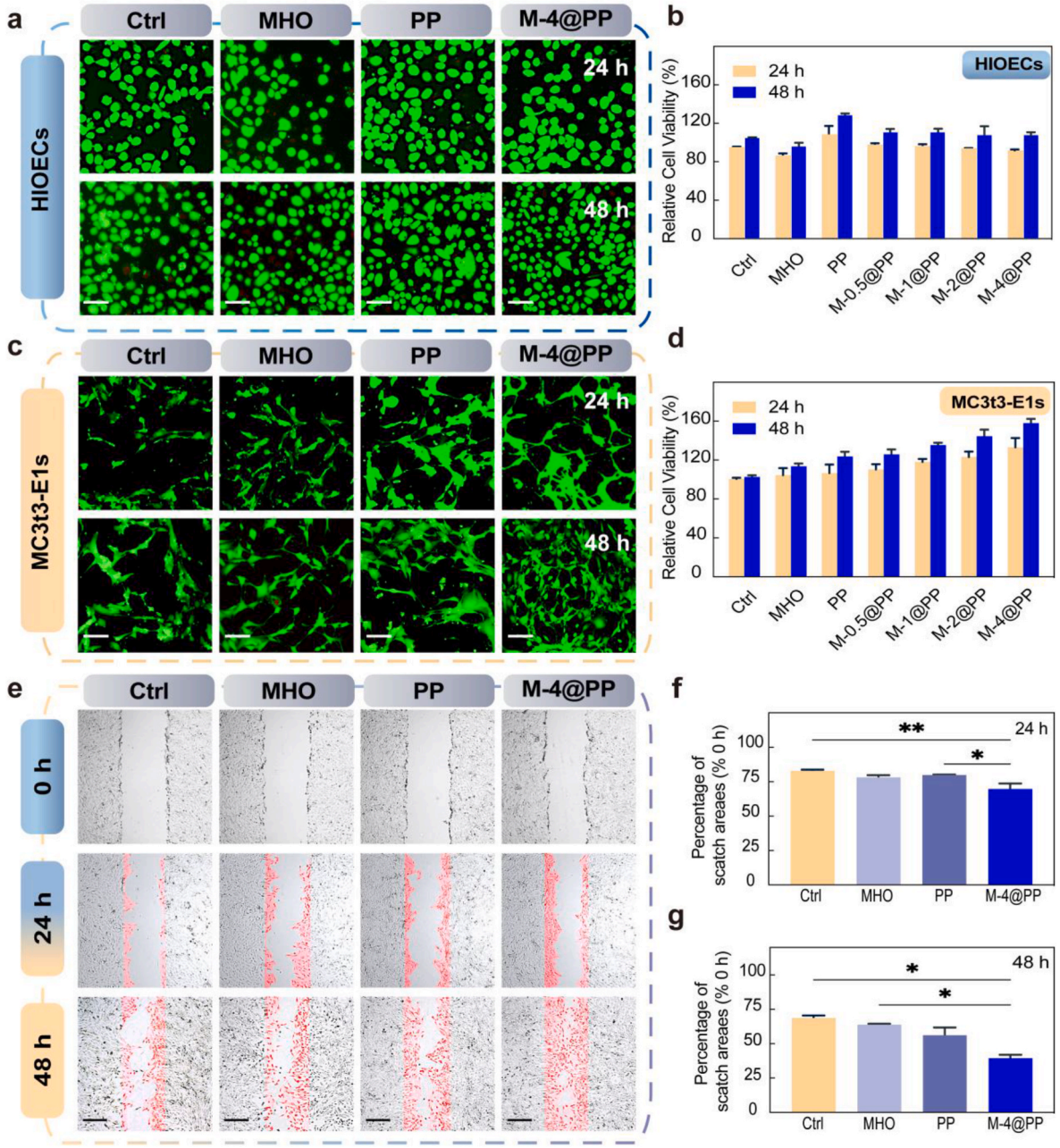

Fig. 4. Effects of the M@PP hydrogel on cytocompatibility and bioactivity
(a) Live/dead tests of HIOECs co-cultured with MHO, PP and M-4@PP groups (5 mg mL^{-1}, n = 3) are performed at 24 h and 48 h using Calcein/PI double fluorescent dye staining. Scale bar: 100 μm. (b) Cell viabilities of HIOECs co-cultured with MHO, PP, M-0.5@PP, M-1@PP, M-2@PP, and M-4@PP groups (5 mg mL^{-1}, n = 3) have been assessed by CCK-8 staining after 24 h and 48 h. (c) Live/dead assays of MC3t3-E1s co-cultured with MHO, PP and M-4@PP groups (5 mg mL^{-1}, n = 3) are performed at 24 h and 48 h using Calcein/PI double fluorescent dye staining. Scale bar: 100 μm. (d) Cell viabilities of MC3t3-E1s co-cultured with MHO, PP, M-0.5@PP, M-1@PP, M-2@PP, and M-4@PP groups (5 mg mL^{-1}, n = 3) have been assessed by CCK-8 staining after 24 h and 48 h. (e) MC3t3-E1s migration after 24 h and 48 h of incubation with leaching solution of MHO, PP, and M-4@PP hydrogels (5 mg mL^{-1}, n = 3). Scale bars measure 200 μm. (f–g) The percentage of scratch regions of MC3t3-E1s following incubation with leaching solution of MHO, PP, and M-4@PP hydrogels (5 mg mL^{-1}, n = 3, $*p < 0.05$, and $**p < 0.01$) for 24 h and 48 h.

M-0.5@PP, M-1@PP, M-2@PP, and M-4@PP at concentrations ranging from 1.25 to 20 mg mL^{-1} is found to be between 123.65 % and 157.95 % for MC3t3-E1s, and between 100.13 % and 127.26 % for HIOECs (Fig. 4b and d, S10). Notably, HIOECs viability decreases slightly at higher minocycline concentrations, with about 80 % of cells surviving after 24 h in a 20 mg mL^{-1} MHO solution (Fig. S10). This reduction in viability is likely due to excessive minocycline release, implying an overdose from clinical pharmaceutical carriers could lead to undesirable side effects.

We assess the capacity of hydrogels to enhance MC3t3-E1 cell migration, finding that the M-4@PP group's gap area is almost closed within 48 h (Fig. 4e–g). The residual scratch area treated with M-4@PP hydrogel show a 1.96-fold increase in growth compared to the control group (31.39 %) (Fig. 4g). The enhanced cell migration of M-4@PP is due to the functional groups (catechol and quinone), which improve cell adhesion and proliferation by interacting with tissue surfaces and mimicking the extracellular matrix [46].

We further investigate the expression of genes related to epithelial junction integrity, focusing on ZO-1 (Zonula Occludens-1) and E-

cadherin (Epithelial Cadherin), which are essential for maintaining the gingival junctional epithelium. Both PP and M-4@PP groups display high expression levels of these genes (Fig. S11). RUNX-2 (Runt-related transcription factor 2) regulates a number of genes involved in bone matrix development, including COL-1 (Type I collagen) and OCN (Osteocalcin), both of which are essential for bone matrix formation and bone remodeling [48]. With relative increases of 2.3, 2.0, and 3.8 times, respectively, the RNA expression of RUNX-2, OCN, and COL-1 has considerably greater in the M-4@PP hydrogel compared to the control group. These findings demonstrate that M-4@PP supports cell migration, restores epithelial junctions, and enhances osteogenesis, making it a promising bioadhesive scaffold for periodontal tissue repair.

3.5. *In vivo* therapeutic efficacy of M-4@PP for periodontitis

To evaluate therapeutic potential of M-4@PP hydrogel, a rat periodontitis model has been established by ligating threads and locally inoculating several human periodontal pathogens (Fig. 5a), which accurately representing the microbial dysbiosis occurring in human periodontitis [49]. Fig. 5b indicates the comparative treatment protocols for M-4@PP hydrogel and current clinical therapy (commercial medications, MHO). As noted above, the M-4@PP hydrogel demonstrates the ability to maintain effective medication levels for an extended period, achieving bacterial-killing ratios of *P. gingivalis* up to 98.1 %, surpassing the 88.1 % observed with MHO (Fig. 3b). Additionally, the bioadhesive and mechanical properties of hydrogel provide more reliable pocket retention, resulting in space and time window sufficient for periodontal bone regeneration. Herein, unlike the weekly MHO injection [8], we have implanted the M-4@PP hydrogel just on the first day of therapy, making it a more realistic option for future clinical applications.

H&E staining has been employed to assess the inflammation severity and the state of periodontal tissue. The saline group (Fig. 5c) exhibits disrupted interdental papillae, considerable inflammatory cell infiltration, as well as a substantial reduction in alveolar bone height. By day 28, the gingival margin remains red and swollen (Fig. 5c, gray arrow). In the MHO group, early-stage signs (2–7 d) of gingival recession and slight dark redness have been noted (Fig. 5c, yellow arrow). In contrast, the experimental group exhibits attachment of the junctional epithelium to

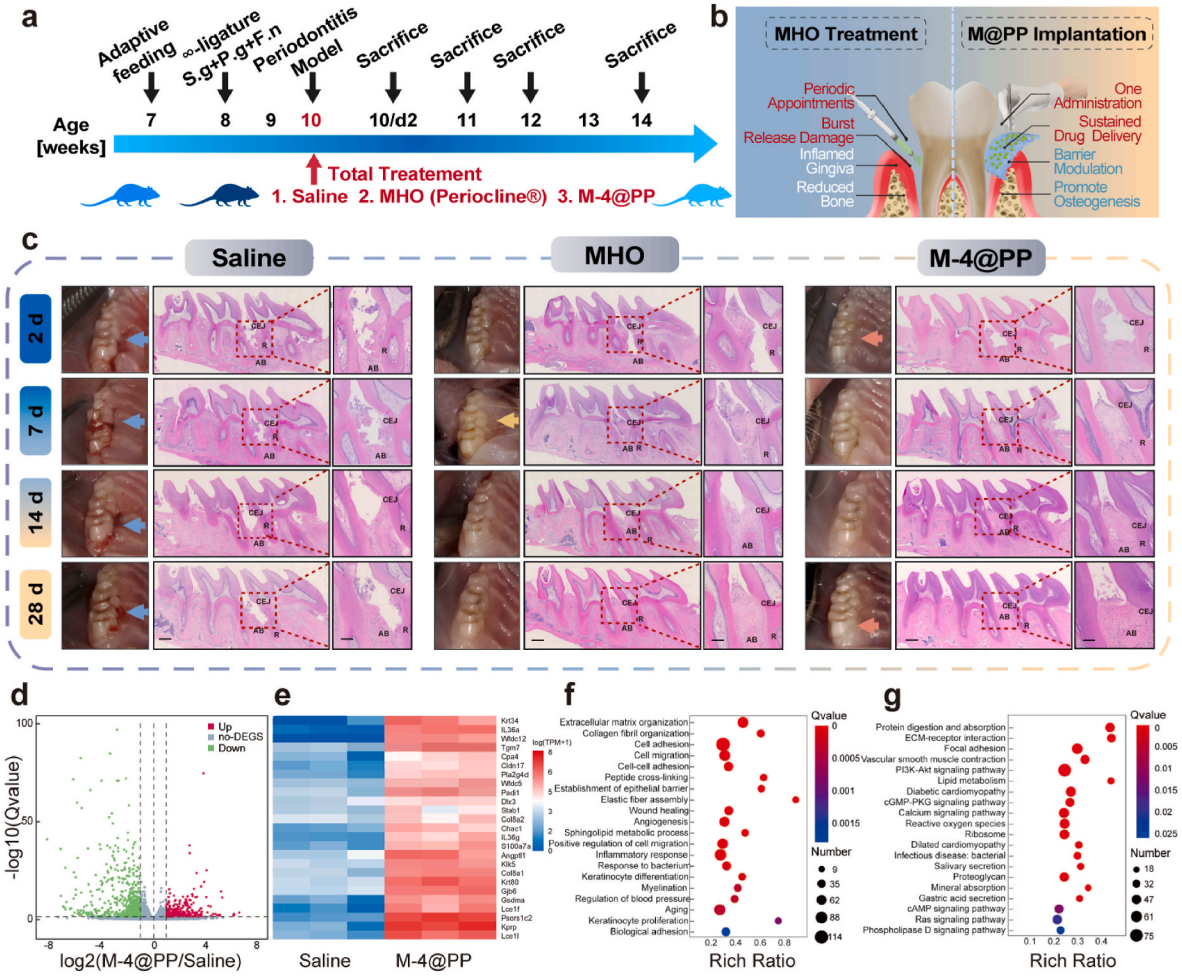

Fig. 5. *In vivo* therapeutic efficacy and potential mechanisms of M-4@PP for periodontitis
(a) The experimental periodontitis is established by placing silk sutures subgingival to the right maxillary first molar and infecting by *P. gingivalis (P.g)*, *F. nucleatum (F.n)*, and *S. gordonii (S.g)* on the SD rat models for 14 d. (b) The comparative treatment protocols for M-4@PP hydrogel and current clinical therapy (commercial medications, MHO). (c) Left: digital photographs of periodontal tissue changes in SD rats after different treatments, blue arrows indicate swelling gingival with BOP (+) (bleeding on probing positive), yellow arrows indicate gingival recession, and pink arrows show reattachment of epithelium. Right: the H&E images of periodontal soft and hard tissues around the maxillary molars after various therapies. CEJ, Cemento-Enamel Junction; R, roots of upper first molars; AB, Alveolar Bone. Scale bars: 250 and 500 μm. (d) Volcano plots of differentially expressed genes (DEGs) between Saline group and M-4@PP group (n = 3), showed the upregulated and downregulated genes. (e) Clustering heatmaps of the DEGs. Red indicates upregulated genes. (f–g) GO enrichment analysis (f) and KEGG pathway enrichment analysis (g) of the DEGs after treatment with saline and M-4@PP group. (For interpretation of the references to color in this figure legend, the reader is referred to the Web version of this article.)

the tooth surface, with no visible plaque deposits (Fig. 5c, pink arrow). Throughout the 4-week therapy, the M-4@PP demonstrates a considerable decrease in probing pocket depth and bleeding index. The attached epithelium strongly adhere to the cemento-enamel junction, accompanied by remarkable bone healing, indicating that the sustained release of minocycline from M-4@PP hydrogel facilitates a superior therapeutic efficacy compared to MHO groups.

3.5.1. Transcriptomic analysis of gingival tissues treated by M@PP

To explore the therapeutic mechanisms of M@PP in periodontitis, RNA sequencing has been performed on gingival tissues from rats treated with saline and M@PP hydrogel (Fig. 5d–e). A total of 2427 genes have been differentially expressed (Q value < 0.05, $|\log2FoldChange| \geq 0$), with 881 upregulated and 1546 downregulated. Gene Ontology (GO) analysis (Fig. 5f) reveals involvement in key processes such as defense response to bacterium, inflammatory response, extracellular matrix organization, angiogenesis, wound healing. The Kyoto Encyclopedia of Genes and Genomes (KEGG) pathway analysis (Fig. 5g) highlights pathways such as ECM-receptor interaction, focal adhesion, PI3K-Akt signaling, and bacterial infection. Promoting macrophage polarization from the pro-inflammatory M1 to the tissue-regenerative M2 phenotype is critical for fostering a regenerative microenvironment in periodontal tissues [50,51]. In the M@PP group, significant activation of the ECM-receptor pathway, essential for immune regulation [52], and the PI3K-Akt pathway, which drives M2 macrophage polarization and epithelial induction [53], highlights its potential for anti-inflammatory effects and macrophage reprogramming. Furthermore, upregulation of inflammation-modulating genes (*S100a7a*, *Pla2g4d*, *Wfdc12*, and *Wfdc5*) suggests enhanced bacterial defense and immune modulation, while genes associated with epithelial barrier repair and tissue regeneration (*Cldn17*, *Gjb6*, *Col8a1*, *Col8a2*, and *Tgm7*) imply M@PP's promise in preventing disease recurrence.

3.5.2. Modulation of the inflammation microenvironment and gingival epithelium integrity

Various histological evaluations were conducted to confirm the expression levels of key proteins involved in regulating the inflammatory response and epithelial barrier recovery, such as TNF-α, iNOS, CD206, E-cadherin, and ZO-1, providing additional evidence for the therapeutic effects of M@PP hydrogels. The periodontitis group exhibits substantially higher M1 marker (iNOS and TNF-α) levels and lower M2 marker (CD206) expression compared to the MHO and M-4@PP groups (Fig. 6a–S12, S13). The M-4@PP group shows the strongest protein inhibition of iNOS (11.33 ± 3.79 %) and TNF-α (176.96 ± 3.7 pg mL^{-1}), as well as the highest protein stimulation of CD206 (30.61 ± 3.79 %) (Fig. 6c and d). This demonstrates M@PP can create a local anti-inflammatory microenvironment by modulating the M2/M1 phenotype.

The gingival junctional barrier maintains epithelial function and microenvironment homeostasis by serving as the first line of defense against periodontal pathogens. Immunoblotting displays that the hydrogel-treated group has considerably higher protein expression levels of ZO-1 (2.29-fold increase) and E-cadherin (1.47-fold increase) compared to the control groups (Fig. 6b). In contrast, the MHO group displays the lowest expression levels for E-cadherin and ZO-1 (0.95-fold and 0.79-fold relative to the saline group, respectively) (Fig. 6e–f), suggesting that minocycline loading may slightly inhibit protein expression in epithelial cells. These results emphasize the value of employing the hydrogel structurally resembling minocycline to minimize the risk of cytotoxicity.

Agar-plate results (Fig. S9) demonstrate a higher proportion of complex bacterial colonies in the control group, while the M-4@PP have significantly reduced bacterial colonies, consistent with quantitative studies from liquid cultures (Fig. 3i). Eliminating the growth and aggregation of periodontal pathogens can inhibit macrophage differentiation into the M1 phenotype, which may alleviate periodontal inflammation and potentially facilitate tissue restoration [50,54]. Collectively, the sustained minocycline release from the inherent bactericidal hydrogel effectively inhibit the formation of periodontal pathogenic biofilms, modulate macrophage subtypes and downregulate the production of pro-inflammatory mediators. Also, the bio-adhesive hydrogel partially restores the epithelial barrier function by promoting the expression of tight and adhesion junction proteins, hence avoiding recurrent periodontitis. However, the precise molecular mechanisms of epithelial junction regeneration remain unknown and require further investigation.

3.5.3. The drug-delivery system M-4@PP hydrogel promotes the repair of damaged hard tissues

In 3D micro-CT reconstructions (Fig. 6g), the M-4@PP hydrogel group displays minimal root surface exposure in the first molar, while the saline group has the most severe bone defects. The distance between the Cemento-Enamel Junction (CEJ, blue line) and the Alveolar Bone Crest (ABC, yellow line) increases in the saline group (Fig. 6h), and the difference become more noticeable over time. Bone volume/total volume (BV/TV), one of the major markers of new bone quality [55], increases significantly by 143.37 % in the M-4@PP hydrogel therapy, reflecting substantial bone reconstruction (Fig. 6i). Research indicates that minocycline can enhance bone formation and promote mineral deposition, resulting in increased trabecular bone density and thickness [56,57]. Compared to the saline group, the M-4@PP group displays higher trabecular number (Tb.N) (up 79.79 %, Fig. 6j), and lower trabecular separation (Tb.Sp) (down 35.33 %, Fig. 6k), whereas the MHO group displays a lower Tb.N and a higher Tb.Sp (increased by 6.11 % and decreased by 1.20 %, respectively). These results suggest that the sustained release of minocycline in the M-4@PP hydrogel enhances osteogenesis more effectively than the burst release observed in the MHO group.

Furthermore, the drug-loaded hydrogels exhibits considerably elevated levels of osteogenic protein markers, with a higher proportion of RUNX2-positive and OCN-positive cells compared to the saline and MHO groups (Fig. 6l). Among these, the M-4@PP hydrogel demonstrates the highest level of RUNX2 expression (25.99 ± 3.79 %) by day 14 (Fig. 6m), OCN expression increases substantially to 30.39 ± 6.94 % by day 28 (Fig. 6n). These findings indicate that, beyond providing anti-inflammatory effects, the drug-loaded hydrogels may also support osteogenesis and bone regeneration.

3.5.4. In vivo biosafety evaluation

We investigate the potential toxicity in the heart, liver, spleen, kidneys, and lungs of rats one-month post-treatment. No significant inflammatory infiltration or pathological changes have been observed in any of these organs (Fig. S14). Analysis of rat serum samples reveals no significant differences in biochemical indicators between the groups (Fig. S15).

4. Conclusion

In summary, this study introduces a cost-effective and easily fabricated dual-network hydrogel drug delivery platform, composed of poly (acrylic acid) and poly(dopamine), which are structurally analogous to minocycline. This dual-network hydrogel achieves high drug loading efficiency and sustained release via hydrogen bonding and electrostatic interactions, and its acidic microenvironment optimizes therapeutic efficacy, while the antioxidant effect of its functional groups ensures the drug-carrying platform excellent anti-inflammatory effect. The M@PP hydrogel demonstrates excellent biocompatibility (100.13–157.95 % cell viability in 48 h), optimal bioadhesion (4.61–11.13 kPa), and exceptional mechanical strength (177.2 kPa), ensuring long-term drug retention in periodontal pockets. By delivering a non-toxic yet effective dosage of minocycline (below 15 μg mL^{-1}), the hydrogel effectively eliminates bacterial biofilm and reinforces the epithelial barrier. Subsequently, the synergistic effect of the hydrogel matrix and sustained

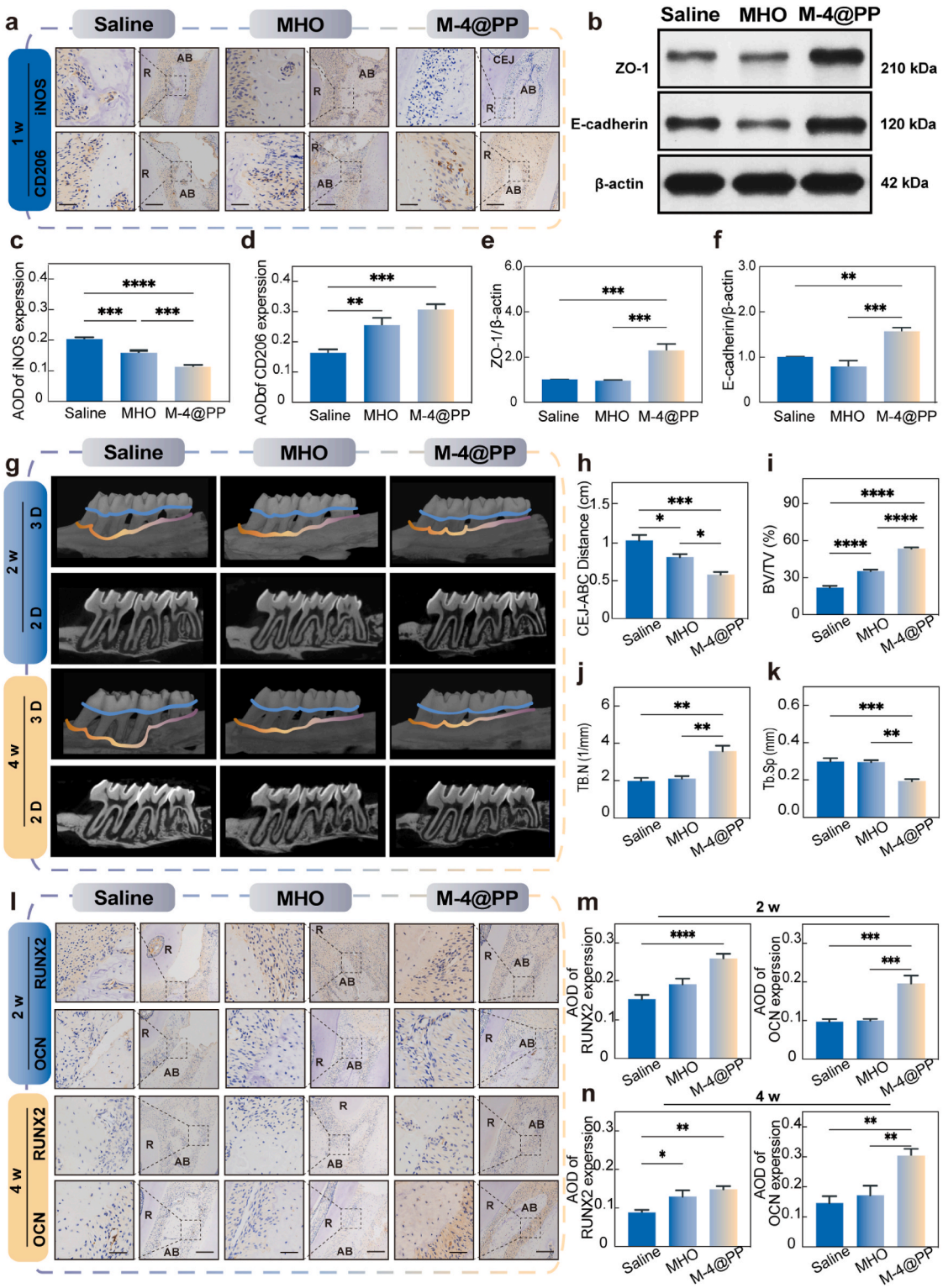

Fig. 6. The M-4@PP hydrogel modulates the inflammation microenvironment, promotes the gingival epithelium integrity recovery and periodontal bone regeneration

(a) Immunohistochemical images of iNOS and CD206 after 7 d of various group treatments, scale bars: 50 and 200 μm. (b) Western blot detection of epithelial integrity-related proteins ZO-1 and E-cadherin, with β-actin as the control. (c–d) The corresponding quantitative analysis of iNOS and CD206 in various groups for 7 d (n = 5, $^{**}p < 0.01$, $^{***}p < 0.001$, and $^{****}p < 0.0001$). (e–f) Semi-quantitative analysis of the protein expression level of ZO-1 and E-cadherin through Image J. (n = 5, $^{**}p < 0.01$, $^{***}p < 0.001$). (g) Micro-CT pictures of maxillary alveolar bone surrounding the right maxillary molars following treatment. Up images show 3D reconstructions, while down images show Mesio-distal Sagittal Slices. The blue lines indicate the Cemento-Enamel Junction (CEJ); the yellow lines indicate Alveolar Ridge Crests (ABC). (h–k) Quantitative analysis of microstructural parameters: CEJ-ABC, BV/TV (Bone volume/total volume), TB.N (trabecular number), and Tb.Sp (trabecular separation). (n = 5, $^{*}p < 0.05$, $^{**}p < 0.01$, $^{***}p < 0.001$, and $^{****}p < 0.0001$). (i) Immunohistochemical images of RUNX2 and OCN in various groups for 2 and 4 w. scale bars: 50 and 200 μm. (m–n) Quantitative study of RUNX2 and OCN in various groups for 2 and 4 w. (n = 5, $^{*}p < 0.05$, $^{**}p < 0.01$, $^{***}p < 0.001$, and $^{****}p < 0.0001$). (For interpretation of the references to color in this figure legend, the reader is referred to the Web version of this article.)

minocycline release maintains a favorable microbial immune environment, thus promoting periodontal bone regeneration. Based on our research, this multifunctional hydrogel not only exemplifies the power of leveraging material interactions to enhance therapeutic approach for periodontitis, outperforming traditional medications, but also has the potential to be extended to design a collection of multifunctional biomaterials for treating various biofilm-related disorders.

CRediT authorship contribution statement

Shiyao Liu: Writing – review & editing, Writing – original draft, Visualization, Validation, Software, Methodology, Investigation, Funding acquisition, Formal analysis, Conceptualization. **Wenqian Zheng:** Writing – review & editing, Writing – original draft, Resources, Methodology, Data curation, Conceptualization. **Lina Wang:** Writing – original draft, Visualization, Methodology, Investigation. **Yajie Zhang:** Visualization, Methodology, Investigation, Data curation. **Kang Feng:** Visualization, Methodology, Investigation. **Yan Zhang:** Visualization, Validation, Methodology. **Haitao Yang:** Methodology, Investigation. **Yao Xiao:** Writing – review & editing, Funding acquisition. **Chenxi Sun:** Software, Investigation. **Xiqiang Liu:** Writing – review & editing, Supervision, Project administration, Funding acquisition, Conceptualization. **Baoyang Lu:** Writing – review & editing, Supervision, Resources, Project administration, Conceptualization. **Xuemin Yin:** Supervision, Resources, Project administration, Conceptualization.

Declaration of generative AI and AI-assisted technologies in the writing process

During the preparation of this work the authors used ChatGPT in order to improve language. After using this tool, the authors reviewed and edited the content as needed and take full responsibility for the content of the publication.

Declaration of competing interest

The authors declare that they have no known competing financial interests or personal relationships that could have appeared to influence the work reported in this paper.

Acknowledgment

This work was supported by the President Foundation of Nanfang Hospital, Southern Medical University (2023B034), National Natural Science Foundation of China (82172752), High Level Introduction of Talent Research Startup Fund, Nanfang Hospital, Southern Medical University, Clinical High-tech and Major Technology Projects in Guangzhou Region (2024P-GX28), and GuangDong Basic and Applied Basic Research Foundation (2023A1515110875).

Appendix A. Supplementary data

Supplementary data to this article can be found online at https://doi.org/10.1016/j.mtbio.2025.101638.

Data availability

Data will be made available on request.

References

[1] X. Tan, S. Liu, X. Hu, R. Zhang, X. Su, R. Qian, Y. Mai, Z. Xu, W. Jing, W. Tian, L. Xie, Near-infrared-enhanced dual enzyme-mimicking Ag-TiO2-x@Alginate microspheres with antibactericidal and oxygeneration abilities to treat periodontitis, ACS Appl. Mater. Interfaces 15 (2023) 391–406, https://doi.org/10.1021/acsami.2c17065.

[2] L. Wu, S. Zhang, L. Zhao, Z. Ren, C. Hu, Global, regional, and national burden of periodontitis from 1990 to 2019: results from the Global Burden of Disease study 2019, J. Periodontol. 93 (2022) 1445–1454, https://doi.org/10.1002/JPER.21-0469.

[3] N.S. Jakubovics, S.D. Goodman, L. Mashburn-Warren, G.P. Stafford, F. Cieplik, The dental plaque biofilm matrix, Periodontol. 2000 86 (2021) 32–56, https://doi.org/10.1111/prd.12361.

[4] E. Choi, H.S. Um, B.S. Chang, S.Y. Lee, J.K. Lee, Clinical and microbiological effects of adjunctive local delivery of minocycline (Periocline®) in patients receiving supportive periodontal therapy: a pilot study, J Periodontal Implant Sci 51 (2021) 53–62, https://doi.org/10.5051/jpis.2002720136.

[5] T. Zhang, Y. Qiu, J. Song, P. Zhou, H. Liao, Y. Cheng, X. Wu, Electrosprayed minocycline hydrochloride-loaded microsphere/SAIB hybrid depot for periodontitis treatment, Drug Deliv. 28 (2021) 620–633, https://doi.org/10.1080/10717544.2021.1902020.

[6] F.R.F. Teles, M.C. Lynch, M. Patel, G. Torresyap, L. Martin, Bacterial resistance to minocycline after adjunctive minocycline microspheres during periodontal maintenance: a randomized clinical trial, J. Periodontol. 92 (2021) 1222–1231, https://doi.org/10.1002/JPER.17-0565.

[7] Y. Wang, J. Deng, T. Zhang, Y. Hua, Y. Wang, Q. Zhang, T. Jiao, C. Li, X. Zhang, A study on the use of phase transition lysozyme-loaded minocycline hydrochloride in the local treatment of chronic periodontitis, ACS Appl. Bio Mater. 5 (2022) 3146–3157, https://doi.org/10.1021/acsabm.2c00079.

[8] O.L. Tan, S.H. Safii, M. Razali, Clinical efficacy of repeated applications of local drug delivery and adjunctive agents in nonsurgical periodontal therapy: a systematic review, Antibiotics (Basel) 10 (2021) 1178, https://doi.org/10.3390/antibiotics10101178.

[9] D. Steinberg, M. Friedman, Sustained-release delivery of antimicrobial drugs for the treatment of periodontal diseases: fantasy or already reality? Periodontol. 2000 84 (2020) 176–187, https://doi.org/10.1111/prd.12341.

[10] A. Mensah, A.M. Rodgers, E. Larrañeta, L. McMullan, M. Tambuwala, J.F. Callan, A.J. Courtenay, Treatment of periodontal infections, the possible role of hydrogels as antibiotic drug-delivery systems, Antibiotics 12 (2023) 1073, https://doi.org/10.3390/antibiotics12061073.

[11] X. Zhao, Y. Yang, J. Yu, R. Ding, D. Pei, Y. Zhang, G. He, Y. Cheng, A. Li, Injectable hydrogels with high drug loading through B-N coordination and ROS-triggered drug release for efficient treatment of chronic periodontitis in diabetic rats, Biomaterials 282 (2022) 121387, https://doi.org/10.1016/j.biomaterials.2022.121387.

[12] Y. Liang, X. Luan, X. Liu, Recent advances in periodontal regeneration: a biomaterial perspective, Bioact. Mater. 5 (2020) 297–308, https://doi.org/10.1016/j.bioactmat.2020.02.012.

[13] J. Li, S. Song, J. Meng, L. Tan, X. Liu, Y. Zheng, Z. Li, K.W.K. Yeung, Z. Cui, Y. Liang, S. Zhu, X. Zhang, S. Wu, 2D MOF periodontitis photodynamic ion therapy, J. Am. Chem. Soc. 143 (2021) 15427–15439, https://doi.org/10.1021/jacs.1c07875.

[14] N. Yan, J. Xu, G. Liu, C. Ma, L. Bao, Y. Cong, Z. Wang, Y. Zhao, W. Xu, C. Chen, Penetrating macrophage-based nanoformulation for periodontitis treatment, ACS Nano 16 (2022) 18253–18265, https://doi.org/10.1021/acsnano.2c05923.

[15] Y. Li, Y. Ma, J. Yu, C. Li, D. Yu, R. Dai, Q. Li, C.Y. Cao, A dual functional polypeptide with antibacterial and anti-inflammatory properties for the treatment of periodontitis, Int. J. Biol. Macromol. 242 (2023) 124920, https://doi.org/10.1016/j.ijbiomac.2023.124920.

[16] T. Lima de Sousa, D. Dourado, J.S. Rodrigues, J. de Souza Rebouças, M.A.J. R. Montes, F.R. Formiga, Treatment of periodontal disease: does drug delivery matter? Front. Bioeng. Biotechnol. 12 (2024) https://doi.org/10.3389/fbioe.2024.1427758.

[17] Z. Hu, X. Lv, H. Zhang, S. Zhuang, K. Zheng, T. Zhou, L. Cen, An injectable gel based on photo-cross-linkable hyaluronic acid and mesoporous bioactive glass nanoparticles for periodontitis treatment, Int. J. Biol. Macromol. 257 (2024) 128596, https://doi.org/10.1016/j.ijbiomac.2023.128596.

[18] Z. Hu, Y. Zhou, H. Wu, G. Hong, M. Chen, W. Jin, W. Lu, M. Zuo, Z. Xie, J. Shi, An injectable photopolymerizable chitosan hydrogel doped anti-inflammatory peptide for long-lasting periodontal pocket delivery and periodontitis therapy, Int. J. Biol. Macromol. 252 (2023) 126060, https://doi.org/10.1016/j.ijbiomac.2023.126060.

[19] J. Zhao, Y. Wei, J. Xiong, H. Liu, G. Lv, J. Zhao, H. He, J. Gou, T. Yin, X. Tang, Y. Zhang, A multiple controlled-release hydrophilicity minocycline hydrochloride delivery system for the efficient treatment of periodontitis, Int. J. Pharm. 636 (2023) 122802, https://doi.org/10.1016/j.ijpharm.2023.122802.

[20] H. Li, X. Wen, X. Gong, Y. Wu, P. Zhao, Y. Zhang, Z. Sha, H. Chang, X. Chen, Facile minocycline deployment in gingiva using a dissolvable microneedle patch for the adjunctive treatment of periodontal disease, Bioeng. Transl. Med. (2024) e10730, https://doi.org/10.1002/btm2.10730.

[21] M.A.M. Subbaiah, N.A. Meanwell, Bioisosteres of the phenyl ring: recent strategic applications in lead optimization and drug design, J. Med. Chem. 64 (2021) 14046–14128, https://doi.org/10.1021/acs.jmedchem.1c01215.

[22] N.A. Meanwell, Applications of bioisosteres in the design of biologically active compounds, J. Agric. Food Chem. 71 (2023) 18087–18122, https://doi.org/10.1021/acs.jafc.3c00765.

[23] Y. Liu, S. Lin, Z. Ding, Y. Li, Y. Tang, J. Xue, Q. Li, P. Li, H. Wang, Pyridine-boryl radical-catalyzed [3π + 2σ] cycloaddition for the synthesis of pyridine isosteres, Chem 10 (2024) 3699–3708, https://doi.org/10.1016/j.chempr.2024.08.010.

[24] H. Yuk, C.E. Varela, C.S. Nabzdyk, X. Mao, R.F. Padera, E.T. Roche, X. Zhao, Dry double-sided tape for adhesion of wet tissues and devices, Nature 575 (2019) 169–174, https://doi.org/10.1038/s41586-019-1710-5.

[25] Y. Gao, J. Chen, X. Han, Y. Pan, P. Wang, T. Wang, T. Lu, A universal strategy for tough adhesion of wet soft material, Adv. Funct. Materials 30 (2020) 2003207, https://doi.org/10.1002/adfm.202003207.
[26] K. Zhang, X. Chen, Y. Xue, J. Lin, X. Liang, J. Zhang, J. Zhang, G. Chen, C. Cai, J. Liu, Tough hydrogel bioadhesives for sutureless wound sealing, hemostasis and biointerfaces, Adv. Funct. Mater. 32 (2022) 2111465, https://doi.org/10.1002/adfm.202111465.
[27] H. Yuk, J. Wu, T.L. Sarrafian, X. Mao, C.E. Varela, E.T. Roche, L.G. Griffiths, C. S. Nabzdyk, X. Zhao, Rapid and coagulation-independent haemostatic sealing by a paste inspired by barnacle glue, Nat. Biomed. Eng. 5 (2021) 1131–1142, https://doi.org/10.1038/s41551-021-00769-y.
[28] R.J. Lamont, H. Koo, G. Hajishengallis, The oral microbiota: dynamic communities and host interactions, Nat. Rev. Microbiol. 16 (2018) 745–759, https://doi.org/10.1038/s41579-018-0089-x.
[29] S.D. Pandey, J.D. Perpich, K.S. Stocke, J.M. Mansfield, Y. Kikuchi, L. Yakoumatos, A. Muszyński, P. Azadi, H. Tettelin, M. Whiteley, S.M. Uriarte, J. Bagaitkar, M. Vickerman, R.J. Lamont, Impact of polymicrobial infection on fitness of Streptococcus gordonii in vivo, mBio 0 (2023) e00658, https://doi.org/10.1128/mbio.00658-23, 23.
[30] W. Zheng, L. Wang, H. Jiao, Z. Wu, Q. Zhao, T. Lin, H. Ma, Z. Zhang, X. Xu, J. Cao, J. Zhong, J. Xu, B. Lu, A cost-effective, fast cooling, and efficient anti-inflammatory multilayered topological hydrogel patch for burn wound first aid, Chem. Eng. J. 455 (2023) 140553, https://doi.org/10.1016/j.cej.2022.140553.
[31] X. Liu, C. Steiger, S. Lin, G.A. Parada, J. Liu, H.F. Chan, H. Yuk, N.V. Phan, J. Collins, S. Tamang, G. Traverso, X. Zhao, Ingestible hydrogel device, Nat. Commun. 10 (2019) 493, https://doi.org/10.1038/s41467-019-08355-2.
[32] J. Wu, J. Deng, G. Theocharidis, T.L. Sarrafian, L.G. Griffiths, R.T. Bronson, A. Veves, J. Chen, H. Yuk, X. Zhao, Adhesive anti-fibrotic interfaces on diverse organs, Nature 630 (2024) 360–367, https://doi.org/10.1038/s41586-024-07426-9.
[33] Y. Wang, Y. Zhang, Y. Yang, M. Jin, S. Huang, Z. Zhuang, T. Zhang, L. Cao, X. Lin, J. Chen, Y. Du, J. Chen, W. Tan, Versatile dopamine-functionalized hyaluronic acid-recombinant human collagen hydrogel promoting diabetic wound healing via inflammation control and vascularization tissue regeneration, Bioact. Mater. 35 (2024) 330–345, https://doi.org/10.1016/j.bioactmat.2024.02.010.
[34] J. Deng, J. Wu, X. Chen, T.L. Sarrafian, C.E. Varela, W. Whyte, C.F. Guo, E. T. Roche, L.G. Griffiths, H. Yuk, C.S. Nabzdyk, X. Zhao, A bioadhesive pacing lead for atraumatic cardiac monitoring and stimulation in rodent and porcine models, Sci. Transl. Med. 16 (2024) eado9003, https://doi.org/10.1126/scitranslmed.ado9003.
[35] L. Wang, L. Duan, G. Liu, J. Sun, M. Shahbazi, S.C. Kundu, R.L. Reis, B. Xiao, X. Yang, Bioinspired polyacrylic acid-based dressing: wet adhesive, self-healing, and multi-biofunctional coacervate hydrogel accelerates wound healing, Adv. Sci. 10 (2023) 2207352, https://doi.org/10.1002/advs.202207352.
[36] W. Li, Y. Zheng, W. Pang, P. Lai, Bio-inspired adhesive hydrogel for wound healing, Biomed, Tech 1 (2023) 65–72, https://doi.org/10.1016/j.bmt.2022.11.009.
[37] J. Li, A.D. Celiz, J. Yang, Q. Yang, I. Wamala, W. Whyte, B.R. Seo, N.V. Vasilyev, J. J. Vlassak, Z. Suo, D.J. Mooney, Tough adhesives for diverse wet surfaces, Science 357 (2017) 378–381, https://doi.org/10.1126/science.aah6362.
[38] S. Correa, A.K. Grosskopf, H. Lopez Hernandez, D. Chan, A.C. Yu, L.M. Stapleton, E. A. Appel, Translational applications of hydrogels, Chem. Rev. 121 (2021) 11385–11457, https://doi.org/10.1021/acs.chemrev.0c01177.
[39] M. Kirchberg, S. Eick, M. Buchholz, A. Kiesow, S. Sarembe, K. Mäder, Extrudates of lipophilic tetracycline complexes: a new option for periodontitis therapy, Int. J. Pharm. 572 (2019) 118794, https://doi.org/10.1016/j.ijpharm.2019.118794.
[40] H. Ruan, Y. Yu, Y. Liu, X. Ding, X. Guo, Q. Jiang, Preparation and characteristics of thermoresponsive gel of minocycline hydrochloride and evaluation of its effect on experimental periodontitis models, Drug Deliv. 23 (2016) 525–531, https://doi.org/10.3109/10717544.2014.929195.
[41] Q. Li, W. He, W. Li, S. Luo, M. Zhou, D. Wu, Y. Li, S. Wu, Band-Aid-like self-fixed barrier membranes enable superior bone augmentation, Adv. Sci. 10 (2023) e2206981, https://doi.org/10.1002/advs.202206981.
[42] Y. Wei, Y. Deng, S. Ma, M. Ran, Y. Jia, J. Meng, F. Han, J. Gou, T. Yin, H. He, Y. Wang, Y. Zhang, X. Tang, Local drug delivery systems as therapeutic strategies against periodontitis: a systematic review, J. Control. Release 333 (2021) 269–282, https://doi.org/10.1016/j.jconrel.2021.03.041.
[43] Y. Ye, L. Zheng, T. Wu, X. Ding, F. Chen, Y. Yuan, G.-C. Fan, Y. Shen, Size-dependent modulation of polydopamine nanospheres on smart nanoprobes for detection of pathogenic bacteria at single-cell level and imaging-guided photothermal bactericidal activity, ACS Appl. Mater. Interfaces 12 (2020) 35626–35637, https://doi.org/10.1021/acsami.0c07784.
[44] H. Liu, X. Qu, H. Tan, J. Song, M. Lei, E. Kim, G.F. Payne, C. Liu, Role of polydopamine's redox-activity on its pro-oxidant, radical-scavenging, and antimicrobial activities, Acta Biomater. 88 (2019) 181–196, https://doi.org/10.1016/j.actbio.2019.02.032.
[45] H. Karkhanechi, R. Takagi, H. Matsuyama, Biofouling resistance of reverse osmosis membrane modified with polydopamine, Desalination 336 (2014) 87–96, https://doi.org/10.1016/j.desal.2013.12.033.
[46] Y. Fu, L. Yang, J. Zhang, J. Hu, G. Duan, X. Liu, Y. Li, Z. Gu, Polydopamine antibacterial materials, Mater. Horiz. 8 (2021) 1618–1633, https://doi.org/10.1039/D0MH01985B.
[47] D.P. Miller, Z.R. Fitzsimonds, R.J. Lamont, Metabolic signaling and spatial interactions in the oral polymicrobial community, J. Dent. Res. 98 (2019) 1308–1314, https://doi.org/10.1177/0022034519866440.
[48] S. Wang, Y. Gong, Z. Wang, X. Meng, Z. Luo, C.J. Papasian, J. Greenbaum, Y. Li, Q. Liang, Y. Chen, X. Li, Q. Xiang, H. Zhang, Y. Liu, L. Cheng, Y. Hu, L. Tan, H. Shen, H. Xiao, H. Deng, Regulon active landscape reveals cell development and functional state changes of human primary osteoblasts in vivo, Hum. Genom. 17 (2023), https://doi.org/10.1186/s40246-022-00448-2.
[49] L. Bai, B. Chen, Y. Liu, W. Zhang, S. Duan, A mouse periodontitis model with humanized oral bacterial community, Front. Cell. Infect. Microbiol. 12 (2022) 842845, https://doi.org/10.3389/fcimb.2022.842845.
[50] R. Nie, Q. Zhang, Z. Feng, K. Huang, C. Zou, M. Fan, Y. Zhang, J. Zhang, J. Li-Ling, B. Tan, H. Xie, Hydrogel-based immunoregulation of macrophages for tissue repair and regeneration, Int. J. Biol. Macromol. 268 (2024) 131643, https://doi.org/10.1016/j.ijbiomac.2024.131643.
[51] S. Yang, Y. Zhu, C. Ji, H. Zhu, A. Lao, R. Zhao, Y. Hu, Y. Zhou, J. Zhou, K. Lin, Y. Xu, A five-in-one novel MOF-modified injectable hydrogel with thermo-sensitive and adhesive properties for promoting alveolar bone repair in periodontitis: antibacterial, hemostasis, immune reprogramming, pro-osteo-/angiogenesis and recruitment, Bioact. Mater. 41 (2024) 239–256, https://doi.org/10.1016/j.bioactmat.2024.07.016.
[52] S. Te, D. Dp, A. Je, The extracellular matrix and the immune system: a mutually dependent relationship, Science (New York, N.Y.) 379 (2023), https://doi.org/10.1126/science.abp8964.
[53] G. Liu, L. Zhang, X. Zhou, J. Xue, R. Xia, X. Gan, C. Lv, Y. Zhang, X. Mao, X. Kou, S. Shi, Z. Chen, Inducing the "re-development state" of periodontal ligament cells via tuning macrophage mediated immune microenvironment, J. Adv. Res. 60 (2023) 233–248, https://doi.org/10.1016/j.jare.2023.08.009.
[54] S. Peng, H. Fu, R. Li, H. Li, S. Wang, B. Li, J. Sun, A new direction in periodontitis treatment: biomaterial-mediated macrophage immunotherapy, J. Nanobiotechnol. 22 (2024) 359, https://doi.org/10.1186/s12951-024-02592-4.
[55] A. Gj, C. Rb, H. Jr, Z. P, Microarchitecture and morphology of bone tissue over a wide range of BV/TV assessed by micro-computed tomography and three different threshold backgrounds, Med. Eng. Phys. 106 (2022) 103828, https://doi.org/10.1016/j.medengphy.2022.103828.
[56] Y. Kim, J. Kim, H. Lee, W. Shin, S. Lee, J. Lee, J. Park, B.H. Jhun, Y. Kim, S. Yi, K. Kim, Tetracycline analogs inhibit osteoclast differentiation by suppressing MMP-9-mediated histone H3 cleavage, Int. J. Mol. Sci. 20 (2019) 4038, https://doi.org/10.3390/ijms20164038.
[57] S. Singh, D. Khanna, S. Kalra, Minocycline and doxycycline: more than antibiotics, Curr. Mol. Pharmacol. 14 (2021) 1046–1065, https://doi.org/10.2174/1874467214666210210122628.